Band Structure, Band Offsets, and Intrinsic Defects Properties of Few-Layer Arsenic and Antimony

Yuanshuang Liu, [†] *Ting Wang,* [†] *John Robertson,*[§] *Jianbin Luo,* [†] *Yuzheng Guo,**[‡] *Dameng Liu,**[†]

[†]State Key Laboratory of Tribology, Tsinghua University, Beijing 100084, China

[‡]College of Engineering, Swansea University, Swansea SA1 8EN, United Kingdom

[§] Department of Engineering, University of Cambridge, Cambridge CB2 1PZ, United Kingdom

E-mail: *Yuzheng.guo@swansea.ac.uk *ldm@tsinghua.edu.cn

ABSTRACT: We present a detailed first-principle study of few-layer arsenic and antimony's electronic structure. The band structure of 2D arsenic and antimony are calculated by hybrid functional with the spin-orbital coupling. The results show that the band gap of arsenene (monolayer arsenic) and antimonene (monolayer antimony) is 1.93eV and 1.52eV, respectively. It is observed that the band gap closes up in tri-layer arsenic and bilayer antimony. The band alignment with HfO_2 and other 2D materials is calculated to show that HfO_2 is a good candidate for gate oxide in field effect transistors. It is found out that point defects such as single vacancy or adatom will introduce several defect states in arsenene in the middle of the band gap. Meanwhile, the defect formation energy becomes negative when Fermi level is close to band edges. By comparison, the defect formation energy in antimonene is always positive so that the Fermi level pinning should be suppressed in contact with reactive metal.

Introduction

Two-dimensional (2D) materials such as graphene and graphene-like materials have been widely used in electronic and photonic devices due to their unique electronic,[1-3] optical,[4-6] and chemical properties.[7] For instance, when materials are thinned to few-layer, the band gap will be increased, showing tuneable electronic properties.[8] Therefore, there is plenty of room for band engineering of these materials.[8-10] However, the electronic properties of 2D semiconductor materials strongly depend on the defect properties.[11] Among various kinds of crystal defects, vacancy and adatom are two of the most common defects in 2D materials. Both vacancy and adatom will directly affect doping in semiconductor energeering.[12, 13] In addition, the Coulomb and stress potential generated by lattice distortion near these point defects will scattercarriers, which will affect the electrical and optical properties. [14]

Recently, 2D materials made of group VA elements have emerged as novel 2D materials with suitable band gaps for optoelectronic devices.[15, 16] Among the group VA elements, arsenic (As) and antimony (Sb) have been paid more attention recently.[17, 18] Monolayer material derived from arsenic and antimony are called arsenene and antimonene.[8] In terms of applications, arsenene and antimonene are good candidates in the field of photodetectors, light emitting diodes, and field effect transistors. [19]

However, point defects are inevitable during growth and fabrication process especially for 2D materials, which will greatly affect the electronic properties of the materials.[20] For instance, it has been found in our previous work that MoS_2-based device's performance is severely affected by the sulfur vacancy which induces Fermi level pinning.[21] Moreover, the introduction of dopant in 2D materials is experimentally difficult and might destabilize the 2D material.[22] Therefore, understanding the formation energy of point defects in arsenene and antimonene is essential for

their potential applications. [23, 24] The intrinsic defects as well as their formation energies are calculated as well as the electronic band structure and the band alignment with other 2D materials and oxides,.

METHOD

In this work, all calculations are performed with plane-wave pseudo potential code VASP.[25] Previously, local or semi-local density functional theory severely underestimate the band gap of semiconductors, which cannot predict the defect formation energy correctly.[21, 26, 27] Besides that, the semi-core states in arsenene and antimonene require the removal of electron self-interaction. Therefore, we supplement DFT calculation with HSE hybrid functional to describe band structures and defect states properly. Spin orbital coupling (SOC) effect was considered for both arsenic and antimony. It was found that SOC effect causes less than 0.02eV band splitting on arsenene, while brings about 13% error on the band gap of antimonene. Taking into account the significant computational cost, SOC will not be included in charged defect calculation.

A $4\times3\times1$ supercell containing 48 atoms was used for arsenene. The lattice constants are 14.2 Å$\times$18.4 Å. The Brillouin zone integration was done with a $3\times3\times1$ Monkhorst-Pack grid for both geometry optimization and electronic properties calculation. In order to reduce the interaction force between layers, a 30 Å vacuum layer was inserted. In the geometry relaxation, total energy convergence criteria is set to be 2×10^{-6} eV per atom. Charge transition states of point defects are also calculated by the same size supercell. Corrections for defect charges and band occupations are applied as in Lany and Zunger.[28] The total energy of the perfect supercell (E_H) and the supercell with a defect (Eq) has been calculated with different charge states. The defect formation energy Hq is then found from[21]

$$H_q(E_F,\mu) = \left[E_q - E_H\right] + q(E_V + \Delta E_F) + \sum_\alpha n_\alpha(\mu_\alpha^0 + \Delta\mu_\alpha) \quad (1)$$

Here, the formation energy of a vacancy in a compound depends on the atomic chemical potentials, corresponding to the vacancy in a charge state. In formula (1), q is the charge which is added into the supercell, while qE_v means the change in fermi level when q is added. α in formula (1) represents a certain type of atoms, so n_α is the number of the atoms and μ_α is the relative chemical potential.

RESULTS AND DISCUSSION

Arsenene and antimonene shares the same honeycomb lattice with graphene. The crystal structure is illustrated in Figure 1(a) and (b). Figure 1(a) illustrates the lattice constant (a)of arsenene and antimonene and Figure 1(b) shows the bond length (d) between two atoms. The calculation method and functional used in this work need to be verified before electronic calculation. Herein Table 1 summarizes the calculated and experimental results of structural parameters of arsenene and antimonene. For arsenene, compared with other calculated results, the maximum error of lattice constant calculated in this work is 2%, while the error of bond length is 3%. For antimonene, the error of lattice constant between experimental and calculated result is 4%, while the error of bond length is only 0.3%. To summarize, the errors of the mentioned structural parameters are all within 5% so that hybrid functional can be adopted to calculate the electronic structure and defects formation energy.

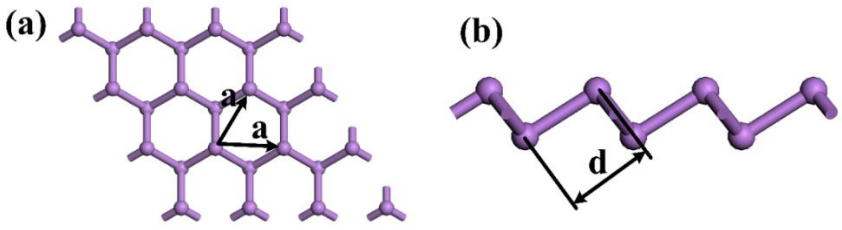

Figure 1. (a) Top view of arsenene (antimonene) (b) Side view of arsenene (antimonene)

Table 1. The comparison of lattice constant (*a*), bond length (*d*) of monolayer arsenic and antimony

	As		Sb	
	a(Å)	d(Å)	a(Å)	d(Å)
GGA	3.64[7]	2.5[19]	4.13[15],4.28[18]	2.88[15]
LDA			4.01[29]	2.84[29]
HSE	3.61[30]	2.51[31]	3.94[19]	2.76[19]
Experiment	--	--	4.13[32]4.5[18]	2.93[18]
This work	3.55	2.42	4.33	2.92

The band structure of monolayer and few-layer arsenic and antimony were calculated and the results as shown in Figure 2 and Figure 3, in which the valence band maximum (VBM) is set to be 0 eV. Figure 2(a) ~ (d) show the band structure of monolayer and few-layer arsenic. For arsenene, it shows semiconductor properties with 1.934eV indirect band gap. When the number of layer added up to bilayer, the band gap decreases rapidly, showing semi metallic properties. When arsenic getting thicker, the band gap closes up. Antimony is similar to arsenic. Monolayer antimonene shows semiconductor electronic properties with an indirect band gap (1.52eV). When antimony turns to be bilayer or bulk, there is no band gap between VBM and conduction band minimum (CBM).

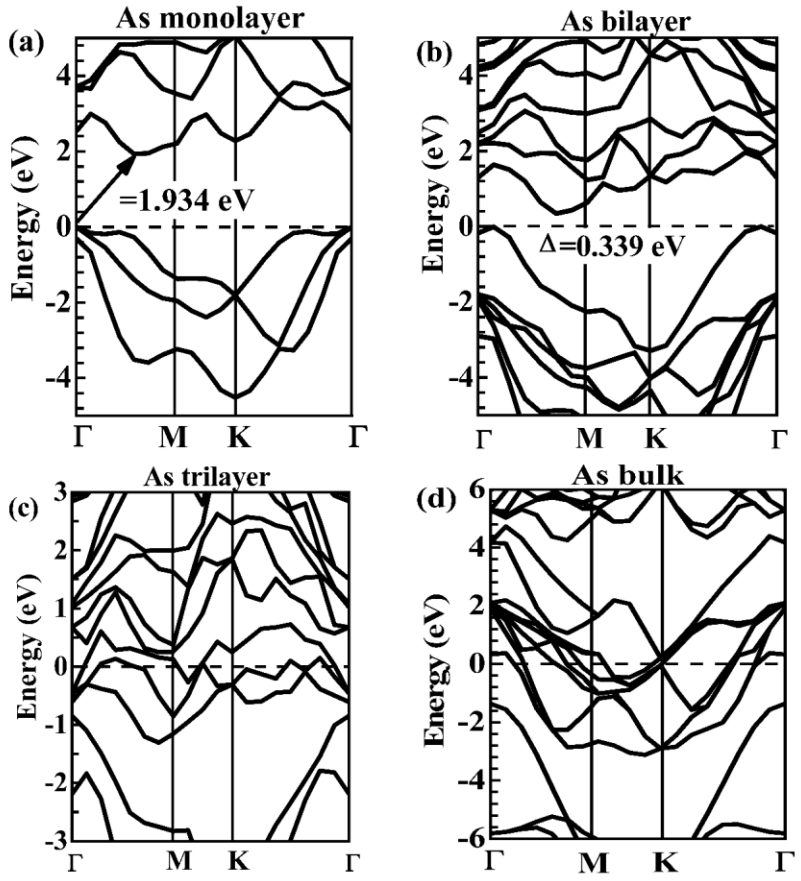

Figure 2. Band structure of monolayer, bilayer, tri-layer, and bulk arsenic calculated by HSE

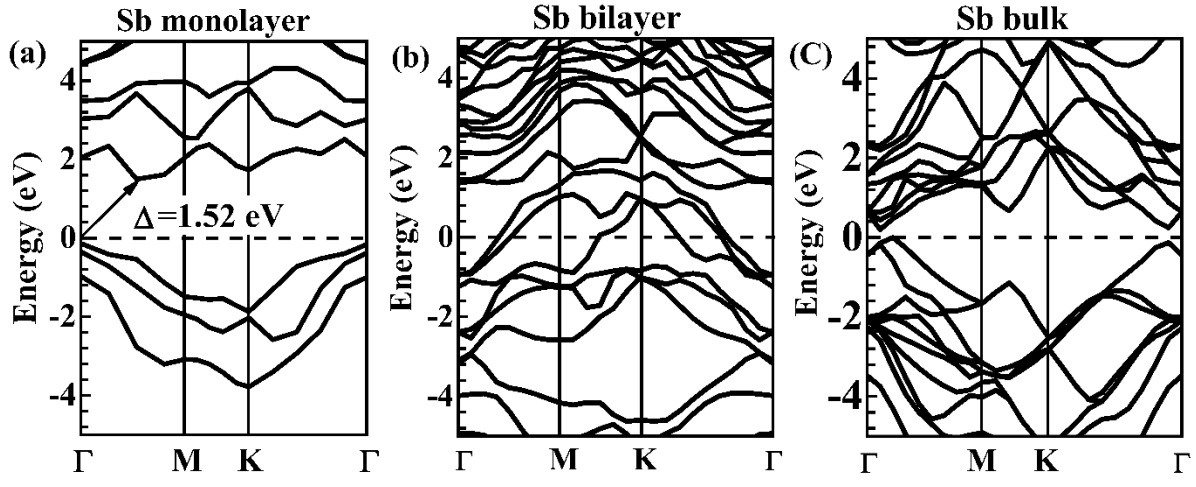

Figure 3. Band structures of monolayer, bilayer, and bulk antimony.

In addition, the calculated results of band gaps of arsenene and antimonene by different kinds of functional are compiled in Table 2. Compared with the hybrid functional, GGA and LDA will underestimate the band gap, while HSE will overestimate the band gap. Although GW and BSE can describe the band structure more accurately, the computational cost is so expensive that much more cores and time will be consumed.

Table 2. The calculated band gaps of arsenene and antimonene by different kinds of functional.

	As		Sb	
	With SOC	Without SOC	With SOC	Without SOC
Functional	Band Gap (eV)		Band Gap (eV)	
HSE06		2.49,[21] 2.2,[33] 2.0,[7] 1.64[34]	1.65,[35] 1.04,[36] 1.4,[37]	2.28,[19] 1.77[19]
LDA			0.76[29]	
GGA		1.52[33]	0.99[15]	1.26[15, 33]
GW	1.3,[38] 2.47[35]		2.38[35]	
BSE	1.6[35]		1.5[35]	
This work	1.929（HSE）	1.934(HSE),	1.52(HSE)	1.72(HSE)
	1.31（GGA）	1.33(GGA)	1.0(GGA)	1.26(GGA)

Furthermore, the band gaps of arsenic and antimony Like the most 2D transition-metal dichalcogenide (TMD) materials, [39-41] the electronic band structure of arsenic and antimony is layer-dependent. The band gap decreases with the increasing number of layers as shown in Figure

4. Such layer-dependent electronic characteristic could be more suitable for photoelectric applications.

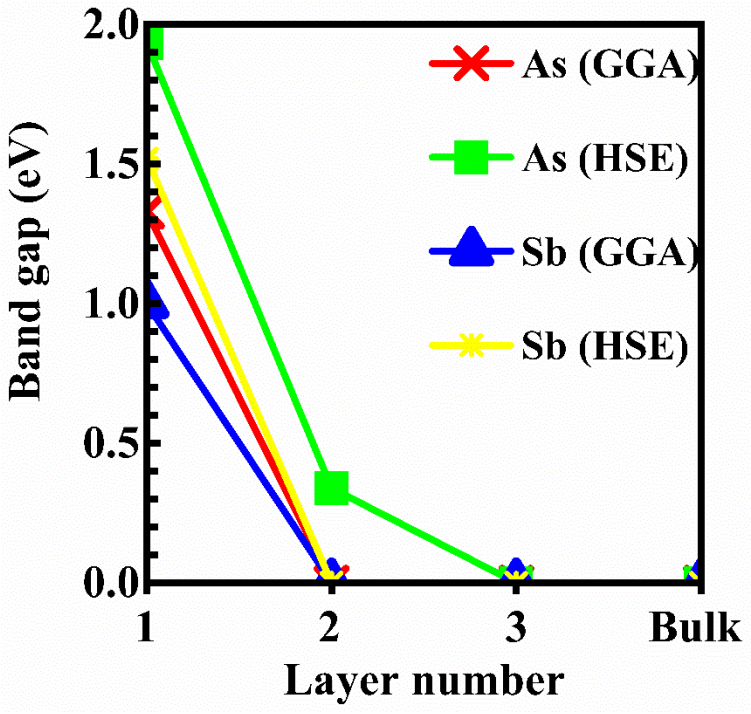

Figure 4. Band gaps calculated by GGA and HSE vs number of layers.

Beside band structure, the effective mass of electron and holes is also calculated in this work. The effective mass of electrons and holes of few-layer arsenic and antimony is derived from quadratic differentiation of CBM and VBM. Therefore, only the effective mass of monolayer and bilayer As as well as monolayer Sb will be calculated. It has been found that smaller effective mass of the holes indicates higher mobility for both p-type and n-type devices[42]. Table 3 shows the effective mass of holes and electrons for different layers of arsenic and antimony. The unit is static electron mass, m_0.

For arsenene, along Γ – M direction, the effective mass of electron and hole were m_h=0.19m_0 and m_e=0.24m_0, which are similar to the results calculated by Zhang *et al*.[19] As for bilayer arsenic,

the electron effective mass increased to m_e=0.29m_0, while the effective mass of holes reduced to m_h=0.048m_0, which means that a higher mobility in bilayer arsenic. For antimonene, the effective mass of electrons and holes was found to be m_h=0.075m_0 and m_e=0.32m_0 along the $\Gamma - M$ direction. The effective masses of arsenic and antimonene calculated in this workare smaller than those of black phosphorene (m_e=1.12m_0) and monolayer MoS_2 (m_e=0.547m_0). [43, 44]

Table 3. The effective mass of holes and electrons for different layers of arsenic and antimony. (Unit: electron mass)

		As	Sb
Monolayer	hole	0.19	0.075
	electron	0.24	0.32
Bilayer	Hole	0.048	——
	Electron	0.29	——

Electron affinity potential (EA) and ionization potential (IP) can describe the ability of materials to gain and lose an electron, which play an essential role in heterojunction optoelectronic devices. The calculated electron affinity and ionization potential of few-layered arsenic and antimony are listed in Table 4.

The charge neutrality levels are listed Table 5. According to our previous calculation in MX_2, vacuum levels are used to align the band edges.[45] The band alignment of arsenene and antimonene with HfO_2 and two other families of 2D materials, MoS_2 and InSe, is plotted in Figure 5. Although arsenene and antimonene have a relatively small electron affinity, HfO_2 is still a good gate insulator for both hole and electron. Arsenene has a slightly higher conduction band than antimonene, which

is also almost the smallest among the stable 2D materials. Considering the high valence band edge, HfS_2/As or HfS_2/Sb will form type II heterostructure, which could be a good candidate for tunnel FET application.

Table 4. Ionization potential and electron affinity of different layers of arsenic and antimony.

	As		Sb	
Layer number	IP	EA	IP	EA
1L	5.28	3.35	5.07	3.55
2L	5.40	3.47	4.42	4.42
3L	5.29	5.29	4.37	4.37
Bulk	5.41	5.41	-3.88	-3.88

Table 5. CNL of arsenic and antimony (HSE).

	As-1L(E_g = 1.934)	As-2L(E_g =0.339)	Sb-1L(E_g =1.52)
CNL (eV)	-3.49	1.72	-2.53

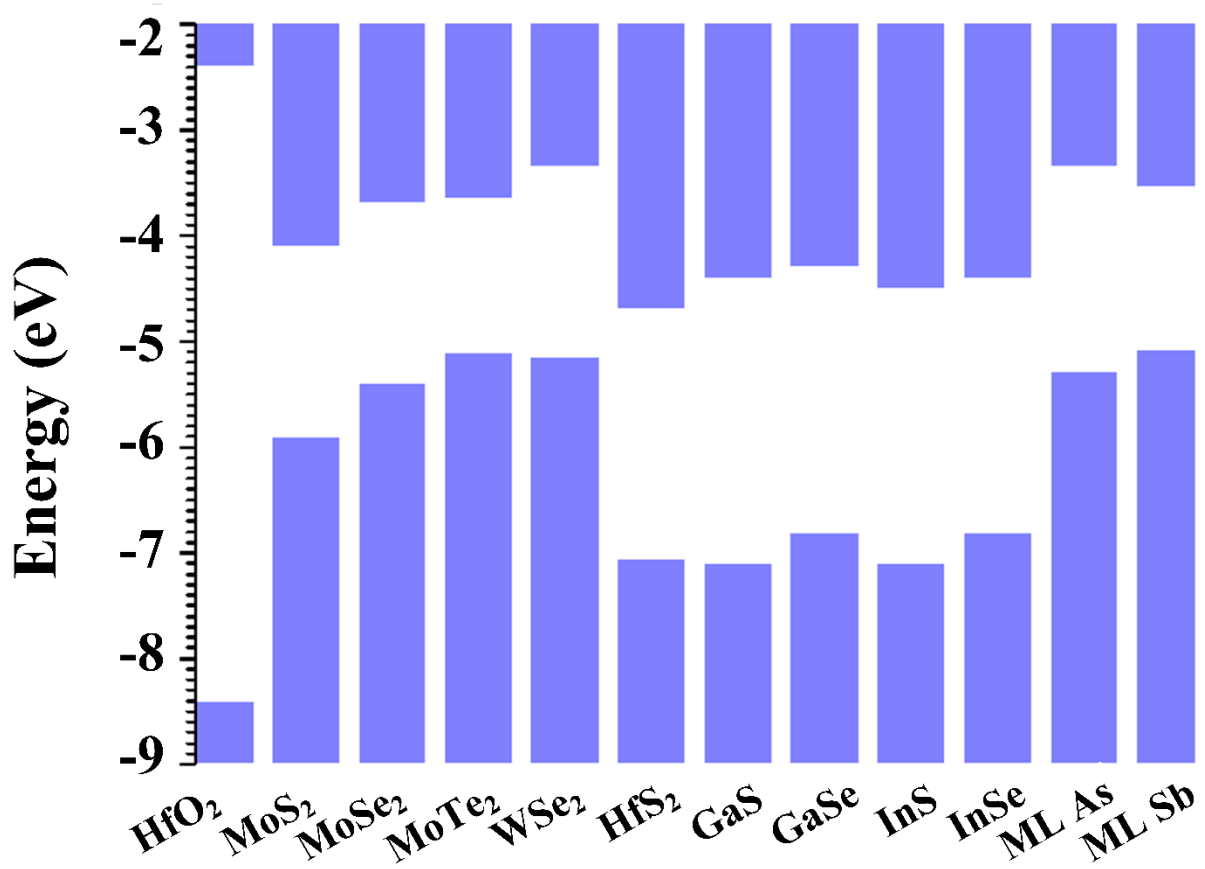

Figure 5. The band alignment of arsenene and antimonene with HfO_2 and other 2D materials.

The previous studies have shown that the point defects can change the electronic properties on 2D materials.[43, 46] Here, we have investigated the electronic properties of vacancy defect and adatom defect.

The density of state of defect supercell of arsenene and antimonene were also calculated as shown in Figure 6 and 7. As illustrated in Figure 6(a), the vacancy defect states in arsenene induces four defect states in the middle of band gap region, one is near the VBM and the other three defect states are very close to the CBM. Meanwhile, vacancy defects lower the VBM as well as the CBM. While adatom induces only one defect state near the CBM and reduces the band gap as shown in

Figure 6(b). The isovalue surface of the electron density for vacancy defects is shown in Figure 6 (c) -(f) , while the isovalue surface of adatom defect is illustrated in Figure 6(g)-(h). No matter it is vacancy or interstitial defect, the higher electronic density of state is mainly distributed around the defect. Yellow indicates that the electron is spin up, while the blue indicates that the electron is spin down.

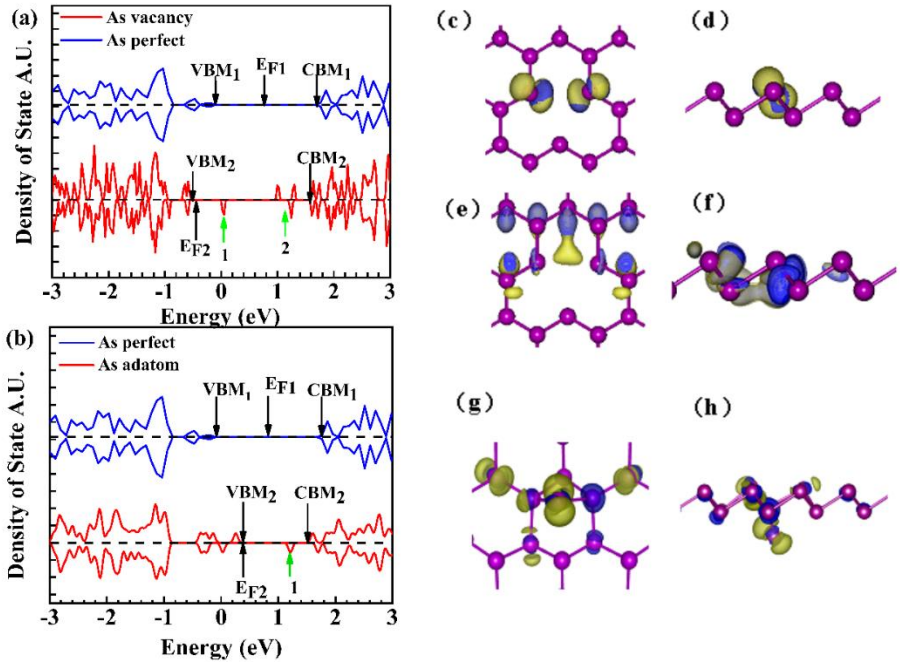

Figure 6. The density of state of (a) arsenene vacancy defect calculated by HSE (b) arsenene adatom defect calculated by HSE. (c) Orbital of the defect states of arsenene vacancy defect (peak 1, front view) (d) Orbitals of the defect states of arsenene vacancy defect (peak 1, side view) (e) Orbital of the defect states of arsenene vacancy defect (peak 2, front view, yellow-spin up, blue-spin down) (f) Orbitals of the defect states of arsenene adatom defect (peak 2, side view, front view, yellow means spin up, blue means spin down) (g) Orbital of the defect states of arsenene adatom defect (front view, front view, yellow means spin up, blue means spin down) (h) Orbital of the defect states of arsenene adatom defect (side view, front view, yellow-spin up, blue-spin down)

Figure 7 shows the defect density of state and insovalue surface of in antimonene. Compared with arsenene, there is only one vacancy defect state in antimonene, located near the CBM. While adatom defect induces two defect states in band gap, one is below the fermi level as well as higher than the VBM and the other one is close to the CBM. In contrast to arsenene, there is spin up electron in antimonene which is shown in Figure 7(c)-(h). As shown in Figure 7(c)-(d), single vacancy defect does not break the three-fold symmetry of antimonene. As for the adatom defect, electrons are mostly located around the extra Sb atom.

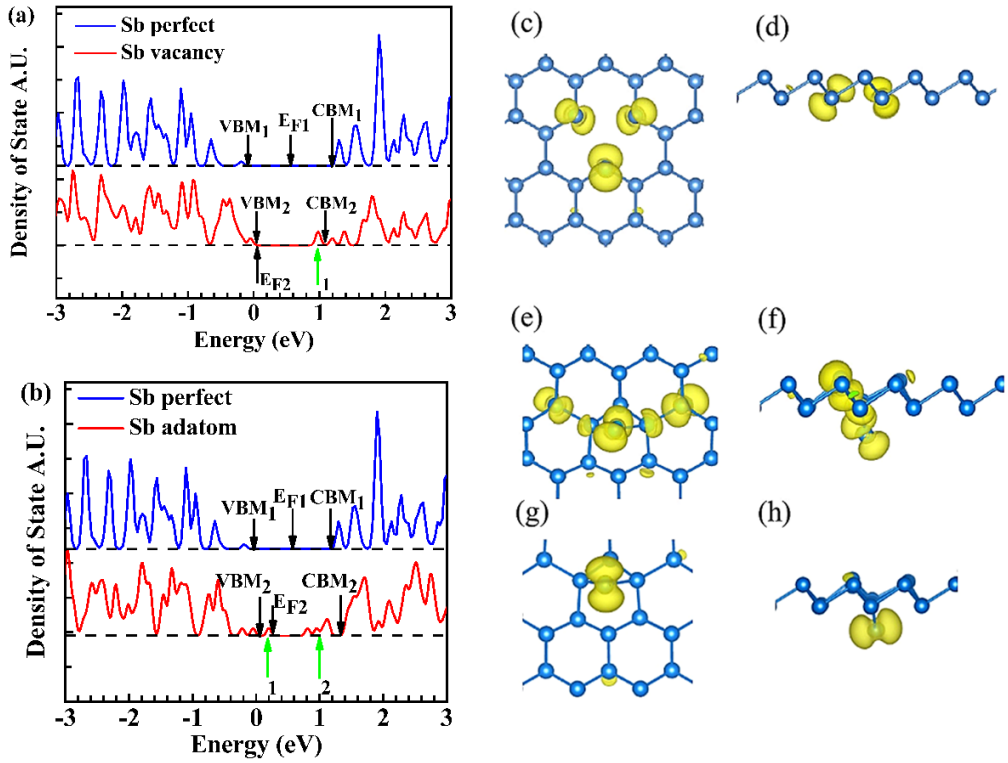

Figure 7. The density of state of (a) antimonene vacancy defect (b) arsenene adatom defect (c) Orbital of the defect states of antimonene vacancy defect (front view) (d) Orbitals of the defect states of arsenene vacancy defect (side view) (e) Orbital of the defect states of antimonene adatom defect (peak 1, front view) (f) Orbitals of the defect states of antimonene adatom defect (peak 1, side view) (g) Orbital of the defect states of antimonene adatom defect

(peak 2, front view) (h) Orbital of the defect states of antimonene adatom defect (peak 2, side view)

Figure 8 shows the vacancy and adatom defect formation energies of arsenene, which is as a function of fermi level. For vacancy defect, only -3 charge state exhibit negative E_f when fermi level is located near CBM as shown in Figure 8(a). Except for -3 charge state, the formation energy of vacancy defect in other charge states is larger than 0 eV. Combined with the ionization potential as shown in Table 4, a vacancy will be formed spontaneously when arsenene in contact with metals with small work functional such as Ti and Sc. Besides, as shown in Figure 8(a), there are quite a few transition levels in the lower and mid gap regions, suggesting p-type doping and deep levels in the band gap induced by vacancy. Such p-type doping will severely affect the performance of arsenene-based devices. Similar to the single vacancy defect, the formation energy of adatom as shown in Figure 8(b) becomes negative when Fermi level is close to CBM and VBM. So when arsenene is in contact with metals that have a higher work function such as Pt and Pd, or metals with low work function such as Ti and Sc, the adatom defect will be formed spontaneously. In addition, the same as vacancy defects, adatom defects will also cause deep levels in the band gap.

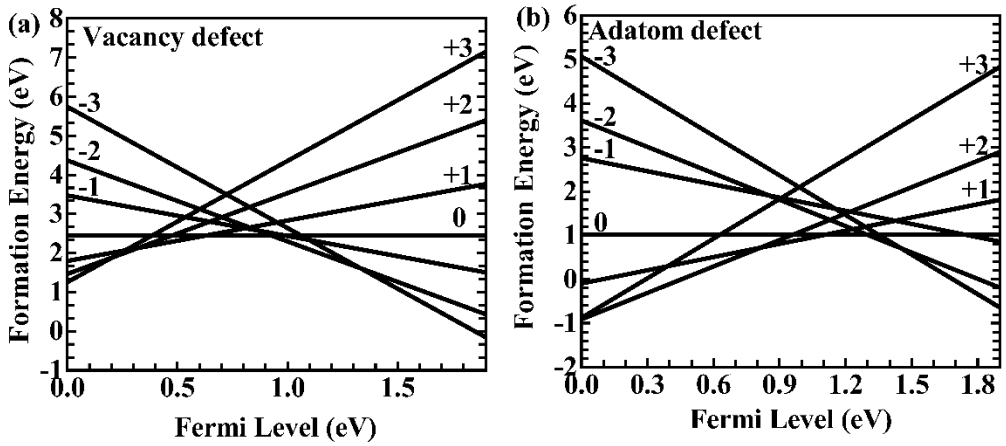

Figure 8. Calculated both vacancy and adatom defect formation energies of Arsenic as a function of the Fermi level. (a) Vacancy defect by using the HSE method (b) Adatom defect by using HSE

Formation energies of vacancy and adatom defects in antimonene are shown in Figure 9, showing that all of the charge states in both vacancy and adatom defect have formation energies larger than 1.5 eV, indicating that both vacancy and adatom defect cannot be formed spontaneously. Compared with arsenene, antimonene has a higher formation energy in all charge states. Figure 9(a) shows that when the vacancy defect in antimonene as an acceptor, the transition level (-1/-3) stays at 1.12eV, forming a deep negative-U level. However, in positive charge states, vacancy defect in antimonene acts as a shallow donor, with +3 charge as the most stable state. It is notable in Figure 9(b) that when adatom defect acts as a donor, the transition levels stay at 0.1eV (+2/0) and 0.25eV (+1/0) above the VBM, which also causes a negative-U level and induces a deep level at the higher region of the band gap. Furthermore, due to antimonene's higher formation energy, it is harder to form the defect levels in band gap region. Thus, antimonene will have fewer defect states in the band gap induced by intrinsic defects and less Fermi-level pinning when in contact with metal.

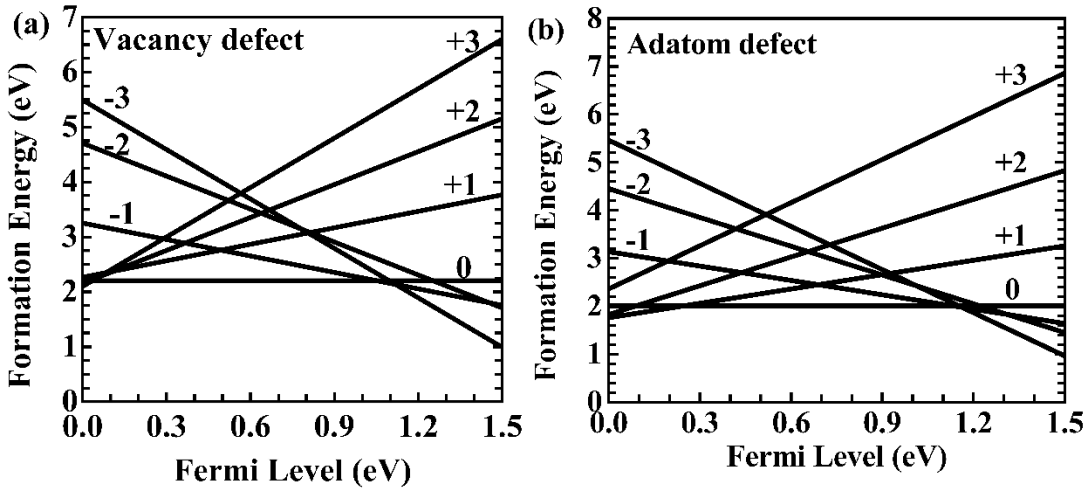

Figure 9. Calculated both vacancy and adatom defect formation energies of antimony as a function of the Fermi level. (a) Vacancy defect (b) Adatom defect.

CONCLUSION

In conclusion, the structural and electronic properties of vacancy and adatom defects in few-layer arsenic and antimony have been investigated by hybrid functional. Antimonene with intrinsic points has a higher formation energy than that in arsenene in different charge state. Besides, the intrinsic defects in antimonene introduce fewer gap states than those in arsenene. The Fermi level pinning in antimonene should be suppressed compared with arsenene due to the positive formation energy of intrinsic defects.

AUTHOR INFORMATION

Corresponding Authors

E-mail: *Yuzheng.guo@swansea.ac.uk, **ldm@tsinghua.edu.cn

Author Contributions

Yuzheng Guo and Dameng Liu designed the calculation experiment and revised the manuscript. Yuanshuang Liu performed experiments and analysis and wrote the manuscript. John Robertson and Jianbin Luo provided theoretical support. Ting Wang proofread the data.

ACKNOWLEDGMENT

Dameng Liu acknowledges financial support from National Science Foundation of China (grant No 51527901, 51575298 and 11890672). Ting Wang acknowledges National Science Foundation of China (grant No 51705284). And we are also grateful to Supercomputing Wales.

ASSOCIATED CONTENT

Supporting Information

Supporting Information Available: The results of electronic band structure, density of state and defect formation energy of arsenic and antimony are calculated by GGA. The band alignment of arsenene and antimonene with other 2D materials is compiled in Table 1 in SI. This material is available free of charge via the Internet at http://pubs.acs.org.

REFERENCES

1. Asadi, M.; Kim, K.; Liu, C.; Addepalli, A. V.; Abbasi, P.; Yasaei, P.; Phillips, P.; Behranginia, A.; Cerrato, J. M.; Haasch, R. Nanostructured Transition Metal Dichalcogenide Electrocatalysts for CO_2 Reduction in Ionic Liquid. *Science* **2016,** *353*, 467-470.
2. Li, F.; Zhao, S.-F.; Chen, L.; Khan, A.; MacFarlane, D. R.; Zhang, J. Polyethylenimine Promoted Electrocatalytic Reduction of CO_2 to CO in Aqueous Medium by Graphene-Supported Amorphous Molybdenum Sulphide. *Energy Environ.* **2016,** *9*, 216-223.
3. Li, F.; Xue, M.; Li, J.; Ma, X.; Chen, L.; Zhang, X.; MacFarlane, D. R.; Zhang, J. Unlocking the Electrocatalytic Activity of Antimony for CO_2 Reduction by Two-Dimensional Engineering of the Bulk Material. *Angew. Chem.* **2017,** *129*, 14910-14914.
4. Meng, B.; Ren, Y.; Liu, J.; Jakle, F.; Wang, L. p-π Conjugated Polymers Based on Stable Triarylborane with n-Type Behavior in Optoelectronic Devices. *Angew. Chem.* **2018,** *130*, 2205-2209.
5. Zhang, S.; Zhou, W.; Ma, Y.; Ji, J.; Cai, B.; Yang, S. A.; Zhu, Z.; Chen, Z.; Zeng, H. Antimonene Oxides: Emerging Tunable Direct Bandgap Semiconductor and Novel Topological Insulator. *Nano Lett.* **2017,** *17*, 3434-3440.
6. Yang, W. S.; Park, B.-W.; Jung, E. H.; Jeon, N. J.; Kim, Y. C.; Lee, D. U.; Shin, S. S.; Seo, J.; Kim, E. K.; Noh, J. H. Iodide Management in Formamidinium-Lead-Halide–Based Perovskite Layers for Efficient Solar Cells. *Science* **2017,** *356*, 1376-1379.
7. Zhu, Z.; Guan, J.; Tománek, D. Strain-Induced Metal-Semiconductor Transition in Monolayers and Bilayers of Gray Arsenic: A Computational Study. *Phys. Rev. B* **2015,** *91*, 161404.
8. Pumera, M.; Sofer, Z. 2D Monoelemental Arsenene, Antimonene, and Bismuthene: Beyond Black Phosphorus. *Adv. Mater* **2017,** *29*, 1605299.
9. Zhang, S.; Guo, S.; Chen, Z.; Wang, Y.; Gao, H.; Gomez-Herrero, J.; Ares, P.; Zamora, F.; Zhu, Z.; Zeng, H. Recent Progress in 2D Group-VA Semiconductors: From Theory to Experiment. *Chem. Soc. Rev.* **2018,** *47*, 982-1021.
10. Zhang, S.; Xie, M.; Li, F.; Yan, Z.; Li, Y.; Kan, E.; Liu, W.; Chen, Z.; Zeng, H. Semiconducting Group 15 Monolayers: A Broad Range of Band Gaps and High Carrier Mobilities. *Angew. Chem.* **2016,** *128*, 1698-1701.
11. Jiang, Y.; Chen, Z.; Han, Y.; Deb, P.; Gao, H.; Xie, S.; Purohit, P.; Tate, M. W.; Park, J.; Gruner, S. M. Electron Ptychography of 2D Materials to Deep Sub-Ångström Resolution. *Nature* **2018,** *559*, 343.

12. Suzuki, Y.; Cardone, G.; Restrepo, D.; Zavattieri, P. D.; Baker, T. S.; Tezcan, F. A. Self-Assembly of Coherently Dynamic, Auxetic, Two-Dimensional Protein Crystals. *Nature* **2016,** *533*, 369.
13. Yang, Y.; Chen, C.-C.; Scott, M.; Ophus, C.; Xu, R.; Pryor, A.; Wu, L.; Sun, F.; Theis, W.; Zhou, J. Deciphering Chemical Order/Disorder and Material Properties at the Single-Atom Level. *Nature* **2017,** *542*, 75.
14. Perez, J. G.; Konya, Z.; Kukovecz, A. Acetone Improves the Topographical Homogeneity of Liquid Phase Exfoliated Few-Layer Black Phosphorus Flakes. *Nanotechnology* **2018**, 29, 365303.
15. Sun, X.; Liu, Y.; Song, Z.; Li, Y.; Wang, W.; Lin, H.; Wang, L.; Li, Y. Structures, Mobility and Electronic Properties of Point Defects in Arsenene, Antimonene and an Antimony Arsenide Alloy. *J. Mater. Chem. C* **2017,** *5,*4159-4166.
16. Li, L.; Yu, Y.; Ye, G. J.; Ge, Q.; Ou, X.; Wu, H.; Feng, D.; Chen, X. H.; Zhang, Y. Black Phosphorus Field-Effect Transistors. *Nat. Nanotechnol.* **2014,** *9*, 372.
17. Rao, C. e. N. e. R.; Sood, A. e. K.; Subrahmanyam, K. e. S.; Govindaraj, A. Graphene: The New Two-Dimensional Nanomaterial. *Angew. Chem.* **2009,** *48*, 7752-7777.
18. Ares, P.; Aguilar-Galindo, F.; Rodríguez-San-Miguel, D.; Aldave, D. A.; Díaz-Tendero, S.; Alcamí, M.; Martín, F.; Gómez-Herrero, J.; Zamora, F. Mechanical Isolation of Highly Stable Antimonene Under Ambient Conditions. *Adv. Mater* **2016,** *28*, 6332-6336.
19. Zhang, S.; Yan, Z.; Li, Y.; Chen, Z.; Zeng, H. Atomically Thin Arsenene and Antimonene: Semimetal-Semiconductor and Indirect-Direct Band-Gap Transitions. *Angew. Chem.* **2015,** *54*, 3112-3115.
20. Zhou, Q.; Liu, S.; Gan, L.; Leng, X.; Su, W. Electronic Properties of the Passive Films Growth on Cu-Ni Alloy from the Viewpoint of Point Defect Model and Power-Law Model. *Mater. Res. Express* **2018,** *5*, 116534.
21. Liu, D.; Guo, Y.; Fang, L.; Robertson, J. Sulfur Vacancies in Monolayer MoS_2 and Its Electrical Contacts. *Appl. Phys. Lett.* **2013,** *103*, 69.
22. Guo, S.; Zhang, Y.; Ge, Y.; Zhang, S.; Zeng, H.; Zhang, H. 2D V-V Binary Materials: Status and Challenges. *Adv. Mater* **2019,** *31*, 1902352.
23. Hu, W.; Wu, X.; Li, Z.; Yang, J. Helium Separation *via* Porous Silicene Based Ultimate Membrane. *Nanoscale* **2013,** *5*, 9062-9066.
24. Leenaerts, O.; Partoens, B.; Peeters, F. M. Graphene: A Perfect Nanoballoon. *Appl. Phys. Lett.* **2008,** *93*, 193107.
25. Becke, A. D. Density-Functional Thermochemistry. III. The Role of Exact Exchange. *J. Chem. Phys.* **1993,** *98*, 5648-5652.
26. Guo, Y.; Robertson, J. Vacancy and Doping States in Monolayer and Bulk Black Phosphorus. *Sci Rep* **2015,** *5*, 14165.
27. Guo, Y.; Liu, D.; Robertson, J. Chalcogen Vacancies in Monolayer Transition Metal Dichalcogenides and Fermi Level Pinning at Contacts. *Appl. Phys. Lett.* **2015,** *106*, 173106.
28. Lany, S.; Zunger, A. Assessment of Correction Methods for the Band-Gap Problem and for Finite-Size Effects in Supercell Defect Calculations: Case Studies for ZnO and GaAs. *Phys. Rev. B* **2008,** *78*, 235104.
29. Wang, G.; Pandey, R.; Karna, S. P. Atomically Thin Group V Elemental Films: Theoretical Investigations of Antimonene Allotropes. *ACS Appl. Mater. Interfaces* **2015,** *7*, 11490-11496.

30. Li, X.-H.; Wang, B.-J.; Cai, X.-L.; Yu, W.-Y.; Zhang, L.-W.; Wang, G.-D.; Ke, S.-H. Arsenene/$Ca(OH)_2$ van der Waals Heterostructure: Strain Tunable Electronic and Photocatalytic Properties. *RSC advances* **2017,** *7*, 44394-44400.
31. Wang, Y.-P; Zhang, C.-W.; Ji, W.-X.; Zhang, R.-W.; Li, P.; Wang, P.-J.; Ren, M.-J.; Chen, X.-L.; Yuan, M. Tunable Quantum Spin Hall Effect *via* Strain in Two-Dimensional Arsenene Monolayer. *J. Phys. D: Appl. Phys.* **2016,** *49*, 055305.
32. Wu, X.; Shao, Y.; Liu, H.; Feng, Z.; Wang, Y. L.; Sun, J. T.; Liu, C.; Wang, J. O.; Liu, Z. L.; Zhu, S. Y.; Wang, Y. Q.; Du, S. X.; Shi, Y. G.; Ibrahim, K.; Gao, H. J. Epitaxial Growth and Air-Stability of Monolayer Antimonene on PdTe2. *Adv Mater* **2017,** *29*, 1605407.
33. Kou, L.; Ma, Y.; Tan, X.; Frauenheim, T.; Du, A.; Smith, S. Structural and Electronic Properties of Layered Arsenic and Antimony Arsenide. *J. Phys. Chem. C* **2015,** *119*, 6918-6922.
34. Kamal, C.; Ezawa, M. Arsenene: Two-Dimensional Buckled and Puckered Honeycomb Arsenic Systems. *Phys. Rev. B* **2015,** *91*, 085423.
35. Wang, Y.; Huang, P.; Ye, M.; Quhe, R.; Pan, Y.; Zhang, H.; Zhong, H.; Shi, J.; Lu, J. Many-Body Effect, Carrier Mobility, and Device Performance of Hexagonal Arsenene and Antimonene. *Chem. Mater.* **2017,** *29*, 2191-2201.
36. Aktürk, O. Ü.; Özçelik, V.O.; Ciraci, S. Single-Layer Crystalline Phases of Antimony: Antimonenes. *Phys. Rev. B* **2015,** *91*, 235446.
37. Zhang, P.; Liu, Z.; Duan, W.; Liu, F.; Wu, J. Topological and Electronic Transitions in a Sb(111) Nanofilm: The Interplay Between Quantum Confinement and Surface Effect. *Phys. Rev. B* **2012,** *85*,201410.
38. Mardanya, S.; Thakur, V. K.; Bhowmick, S.; Agarwal, A. Four Allotropes of Semiconducting Layered Arsenic that Switch into a Topological Insulator *via* an Electric Field: Computational Study. *Phys.Rev.B* **2016,** *94*, 035423.
39. Choi, S.; Shaolin, Z.; Yang, W. Layer-Number-Dependent Work Function of MoS_2 Nanoflakes. *J. Korean Phys. Soc.* **2014,** *64*, 1550-1555.
40. Elías, A. L.; Perea-López, N.; Castro-Beltrán, A.; Berkdemir, A.; Lv, R.; Feng, S.; Long, A. D.; Hayashi, T.; Kim, Y. A.; Endo, M. Controlled Synthesis and Transfer of Large-Area WS_2 Sheets: From Single Layer to Few Layers. *ACS Nano* **2013,** *7*, 5235-5242.
41. Zhao, W.; Ribeiro, R. M.; Toh, M.; Carvalho, A.; Kloc, C.; Castro Neto, A.; Eda, G. Origin of Indirect Optical Transitions in Few-Layer MoS_2, WS_2, and WSe_2. *Nano Lett.* **2013,** *13*, 5627-5634.
42. Fallahazad, B.; Movva, H. C.; Kim, K.; Larentis, S.; Taniguchi, T.; Watanabe, K.; Banerjee, S. K.; Tutuc, E. Shubnikov-de Haas Oscillations of High-Mobility Holes in Monolayer and Bilayer WSe_2: Landau Level Degeneracy, Effective Mass, and Negative Compressibility. *Phys. Rev. Lett.* **2016,** *116*, 086601.
43. Bekaroglu, E.; Topsakal, M.; Cahangirov, S.; Ciraci, S. First-Principles Study of Defects and Adatoms in Silicon Carbide Honeycomb Structures. *Phys. Rev. B* **2010,** *81*, 075433.
44. Han, X.; Stewart, H. M.; Shevlin, S. A.; Catlow, C. R.; Guo, Z. X. Strain and Orientation Modulated Bandgaps and Effective Masses of Phosphorene Nanoribbons. *Nano Lett* **2014,** *14*, 4607-4614.
45. Kim, T.; Seong, T.-Y.; Kwon, O. Investigating the Origin of Efficiency Droop by Profiling the Voltage Across the Multi-Quantum Well of an Operating Light-Emitting Diode. *Appl. Phys. Lett.* **2016,** *108*, 231101.

46. Topsakal, M.; Aktürk, E.; Ciraci, S. First-Principles Study of Two- and One-Dimensional Honeycomb Structures of Boron Nitride. *Phys. Rev. B* **2009,** *79*,115442.

TOC Graphic